Current Optics and Photonics
Vol. 3, No. 5, October 2019, pp. 451-457

ISSN: 2508-7266(Print) / ISSN: 2508-7274(Online)
DOI: https://doi.org/10.3807/COPP.2019.3.5.451

Two-dimensional Laser Drilling Using the Superposition of Orthogonally Polarized Images from Two Computer-generated Holograms

Hwihyeong Lee[1]*, Seongwoo Cha[2], Hee Kyung Ahn[1], and Hong Jin Kong[2]

[1]*Space Optics Team, Advanced Instrumentation Institute, Korea Research Institute of Standards and Science, Daejeon 34113, Korea*
[2]*Department of Physics, Korea Advanced Institute of Science and Technology, Daejeon 34141, Korea*

(Received May 22, 2019 : revised July 29, 2019 : accepted July 30, 2019)

Laser processing using holograms can greatly improve processing speed, by spatially distributing the laser energy on the target material. However, it is difficult to reconstruct an image with arrays of closely spaced spots for laser processing, because the specklelike interference pattern prevents the spots from getting close to each other. To resolve this problem, a line target was divided in two, reconstructed with orthogonally polarized beams, and then superposed. Their optical reconstruction was performed by computer-generated holograms and a pulsed laser. With this method, we performed two-dimensional (2D) laser drilling of polyimide film, with a kerf width of 20 μm and a total processing length of 20 mm.

Keywords : Laser processing, Materials processing, Computer-generated holograms, Diffractive optical element
OCIS codes : (140.3390) Laser materials processing; (090.1760) Computer holography; (050.1970) Diffractive optics

I. INTRODUCTION

Lasers can achieve high intensity when focused onto a small area, because of their coherence and monochromaticity. This property enables the accurate and precise machining of targets of complex shape, without tool wear. With these advantages, the demand for laser processing is increasing in many industries, to fabricate, for example, printed circuit boards, displays, and semiconductors [1]. Conventional laser processing is performed by scanning a single spot on the target material. However, this method limits the processing speed, because the laser has to scan whole paths with a single spot. The speed can be slightly improved by increasing the laser's pulse energy, but the speed remains far below expectation, because the penetrating energy is not proportional to the laser-pulse energy according to the Beer-Lambert Law [2]. At the same time, fluence that exceeds the appropriate value only deteriorates the processing quality, because of transverse heat diffusion. To achieve high quality and a reasonable processing speed corresponding to the laser energy, the laser beam should be spatially distributed on the target material, so that it can process large areas simultaneously. This can be achieved by several methods, such as multiple-beam interference [3, 4], multilens arrays [5, 6], and holograms [7-17]. Among them, the holographic method is very effective, given its high throughput. Many researchers have applied it to patterning [7-11], structuring [12, 13], drilling [14], cutting [15, 16], and welding [17].

In this paper we focus on laser drilling with spots placed very close together, which can be extended to laser cutting. Most previous experiments with holographic laser cutting were performed by scanning multiple spots [15, 16], but this approach is only applicable to periodic cutting patterns, because all spots must be scanned in the same direction. To achieve the highest speed, the scanning process should be minimized by splitting the laser beam into as many spots as possible.

*Corresponding author: hwihyeong@kriss.re.kr, ORCID 0000-0001-8148-7786
Color versions of one or more of the figures in this paper are available online.

There are two requirements for nonscanning laser cutting using holograms. First, the hologram should have a high damage threshold. Since a large number of spots is required for holographic laser cutting, in our case of cutting polyimide with a length of 20 mm, a laser energy of 300 mJ is needed. Dynamic holograms such as spatial light modulators or digital micromirror devices cannot withstand such high energy. Therefore, static holograms made of a material with a high damage threshold, such as fused silica, should be used.

The second requirement is to reduce the specklelike interference that occurs between spots [18, 19]. When a phase-only hologram is reconstructed with a uniform laser beam, highly fluctuating phases occur in the image plane, due to high spatial frequencies. Thus, constructive or destructive interference patterns occur between the spots, causing discontinuity and nonuniformity of the line images. The common solution to this is to temporally average, or accumulate, the various images of the same target [20-23]. However, this method cannot be applied to the present research, because it requires dynamic holograms.

In this study we performed holographic laser processing of polyimide film by using two computer-generated holograms (CGHs) to perform laser drilling with arrays of closely spaced spots. With a limit of laser-pulse energy of 300 mJ, the total cut length was limited to 20 mm. The target pattern had 12 lines distributed in an area of 24 mm × 23 mm, with each line having an average length of about 1.67 mm. If one uses a laser with a pulse energy of several J or more, the cutting length increases linearly, and this can be extended to laser cutting.

The superposition of orthogonally polarized images [24] enabled us to reconstruct multiple continuous line images with static holograms. Based on this method, we designed and fabricated CGHs and demonstrated 2D nonscanning laser processing. In Section 2, we present a method for reducing the interference pattern in the reconstructed image. In Section 3, the algorithm for designing CGHs and parameters for the fabrication of CGHs are demonstrated. In Section 4, the experimental setup and its results are presented. In Section 5 we discuss a practical example for applying this method to laser cutting, and finally we present the conclusions of this research in Section 6.

II. REDUCTION OF INTERFERENCE IN A RECONSTRUCTED IMAGE

The hologram should reconstruct continuous, uniform line images for laser drilling with arrays of closely spaced spots. We summarize a method for reducing the interference pattern in the reconstructed image that can be applied for static holograms, and detailed descriptions can be found in [24]. The hologram can be classified by its reconstructed region and modulation type. We chose Fourier holograms, because they are easy to align and less sensitive to changes in the input-beam intensity. For modulation a phase-only type was adopted, to achieve high efficiency, and to avoid damage to the CGHs by the high-energy laser.

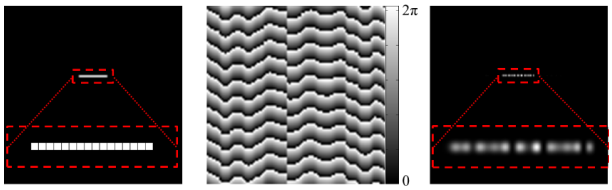

FIG. 1. (a) A line target. (b) A CGH phase made with the target. (c) A reconstructed image. The insets show each of the magnified parts.

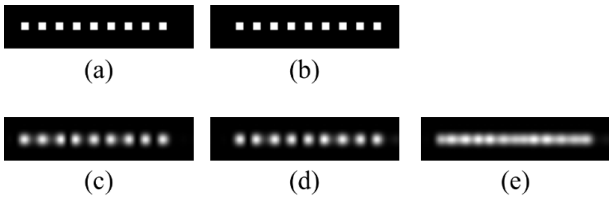

FIG. 2. (a) Divided line target 1. (b) Divided line target 2. (c) Line image numerically reconstructed by target 1. (d) Line image numerically reconstructed by target 2. (e) Superposed image of the reconstructed images.

Figure 1 shows an example of reconstructing a line image with a phase-only Fourier CGH. Figures 1(a) and 1(b) show respectively a line target consisting of 16 spots, and a CGH phase designed by the target. Figure 1(c) shows an image reconstructed from the CGH. It contains a highly fluctuating interference pattern between the spots, which hinders the reconstruction of a continuous line. This is an inherent problem when a phase-only hologram is reconstructed with a uniformly distributed beam.

The first step in reducing the interference pattern is to divide the target into two targets with two-pixel spot intervals, as shown in Figs. 2(a) and 2(b). The second step is to design and fabricate two CGHs corresponding to each divided target, and reconstruct them with orthogonally polarized beams respectively. The reconstructed images have a reduced interference pattern, due to the larger spot interval, as shown in Figs. 2(c) and 2(d). The next step is to superpose them on the same image plane, as shown in Fig. 2(e), and they will be linearly superposed without interference from each other, due to the orthogonal polarizations. Compared to the image produced by a single hologram (Fig. 1(c)), the result shows a much-reduced interference pattern. This method can be easily extended to 2D line images with complex shapes.

III. DESIGN AND FABRICATION OF CGHS

3.1. Optimal-rotation-angle Algorithm for CGH Design

We summarize the optimal-rotation-angle (ORA) algorithm [25] for designing a phase-only CGH. Among the CGH algorithms it shows good performance, with highly uniform spots. Let the 2D discrete complex amplitudes in the image and hologram planes, respectively, be expressed as $a_{mn}\exp(i\psi_{mn})$ and $A_{pq}\exp(i\phi_{pq})$, where a_{mn} and A_{pq} are amplitudes, ψ_{mn} and ϕ_{pq} are phases, and m, n, p, and q are each pixel number. Because we consider a Fourier hologram, they are in Fourier-transform relationship as follows:

$$a_{mn}\exp(i\psi_{mn}) = \sum_{p=0}^{N-1}\sum_{q=0}^{N-1} A_{pq}\exp(i\phi_{pq})\exp\left[i\frac{2\pi}{N}(mp+nq)\right], \quad (1)$$

where N is the number of sampling points, which is assumed to be equal in all directions, without loss of generality. The objective of this algorithm is to optimize the hologram phase ϕ_{pq}, which can reconstruct the target image amplitude a'_{mn} with a given beam amplitude A'_{pq}. Therefore, the amplitudes a_{mn} and A_{pq} before optimization in each plane should converge to a'_{mn} and A'_{pq}, respectively, while ψ_{mn} is a free parameter. This process is performed through a number of iterations. The first iteration begins by Fourier-transforming the hologram's complex amplitude with the randomly given phase ϕ_{pq}, and the given beam amplitude A'_{pq}. When the hologram's phase is changed from ϕ_{pq} to $\phi_{pq}+\Delta\phi_{pq}$, the image amplitude a_{mn} in each pixel is also changed as follows:

$$\Delta a_{mn} = a_{mn}\left[\cos(\omega_{mn,pq}-\Delta\phi_{pq})-\cos(\omega_{mn,pq})\right], \quad (2)$$

where $\omega_{mn,pq}$ is an angle given by

$$\omega_{mn,pq} = \psi_{mn}-\phi_{pq}-\frac{2\pi}{N}(mp+nq). \quad (3)$$

The sum of all of the variations of amplitudes is given by

$$\begin{aligned}\sum_{a_{mn}>0}\Delta a_{mn} &= \cos\Delta\phi_{pq}\sum_{a_{mn}>0} a_{mn}\cos\omega_{mn,pq} \\ &+ \sin\Delta\phi_{pq}\sum_{a_{mn}>0} a_{mn}\sin\omega_{mn,pq} \\ &- \sum_{a_{mn}>0} a_{mn}\cos\omega_{mn,pq} \\ &= C_1\cos\Delta\phi_{pq}+C_2\sin\Delta\phi_{pq}+C_3,\end{aligned} \quad (4)$$

where C_1, C_2, and C_3 are simplified terms of each summation, and $a_{mn}>0$ means that only target spots are considered. Then we can find mathematically the optimal phase change $\Delta\phi_{pq}$ that maximizes the sum of all amplitude variations, as follows:

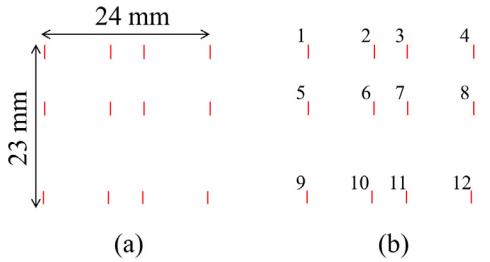

FIG. 3. (a) Target pattern for 2D laser processing. (b) Each line's number.

$$\Delta\phi_{pq} = \begin{cases}\arctan(C_2/C_1) & \text{for } C_1>0 \\ \arctan(C_2/C_1)+\pi & \text{for } C_1<0. \\ (\pi/2)sign(C_2) & \text{for } C_1=0\end{cases} \quad (5)$$

Then ϕ_{pq} is replaced with $\phi_{pq}+\Delta\phi_{pq}$, and the same process is performed for all of the hologram's other pixels. After that, the totally renewed hologram complex amplitude $A_{pq}\exp(i\phi_{pq})$ is Fourier-transformed to obtain the image complex amplitude $a_{mn}\exp(i\psi_{mn})$, and $|a_{mn}|^2$ is compared to the target image intensity $|a'_{mn}|^2$. This is a single iteration; the process is repeated with a newly given image phase ψ_{mn} until the hologram reconstructs a satisfactory image. All CGHs to be described later were designed using the ORA algorithm.

3.2. Design Parameters and Fabrication of CGH

A processing target was determined based on a singulation pattern for a camera module's circuit board, as shown in Fig. 3(a). It consisted of 12 lines in an area of 24 mm × 23 mm, and each line was numbered for easy analysis, as depicted in Fig. 3(b). The length of the upper and middle lines (from 1 to 8) was about 1.7 mm each, and the length of the lower lines (from 9 to 12) was about 1.4 mm each. The line target was divided into two targets, as described in the previous section. The intended kerf width was less than 30 μm, and based on this value the spot size of the reconstructed image was determined to be about 30 μm ($1/e^2$). The size of the fabricated CGH was 17 mm × 17 mm, its pixel pitch 3.4 μm × 3.4 μm, and its number of pixels 5000 × 5000. With these parameters, each divided target had 614 spots and a spot interval of 31.8 μm, while the superposed image had a total of 1228 spots and a spot interval of 15.9 μm.

The fabricated CGH modulated the input beam's phase using the relative difference in depth. The designed phase profile was transferred to the surface of the fused silica by a direct-laser-writing technique [26]. The fabrication process began with spin coating of the photoresist on the substrate. Then, the spot of the UV diode laser scanned the photo-resist, with intensity modulated corresponding to each point. After the development of the photoresist, it was transferred to the fused silica by reactive ion etching. The fabricated CGHs had a diffraction efficiency of about 70%.

IV. EXPERIMENT

4.1. Experimental Setup

Figure 4 shows the experimental setup for the 2D laser drilling using the two CGHs. The light source was a flash-lamp-pumped Nd:YAG laser (Spectra-Physics LAB150) operating in 10-Hz pulsed mode by Q-switching. Its wavelength was 1064 nm, pulse width was about 10 ns, M^2 value was 1.4, and maximum pulse energy was about 300 mJ. The shot-to-shot fluctuation of the laser-pulse energy was 0.7%. The laser beam was expanded twice by the lenses (L1 and L2). A polarizing beam splitter (PBS1) divided the expanded beam into *p*- and *s*-polarized beams, and a half-wave plate (HWP) controlled their splitting ratio. The polarized beams were reflected 90° by mirrors (M1 and M2) that had a dielectric coating for each polarization, and the phase of each beam was modulated by CGH1 and CGH2 respectively. The two beams were combined at PBS2, and optically Fourier transformed by an f-theta lens (FL, Thorlabs FTH254-1064, focal length 254 mm), which minimized aberrations. The two CGHs and PBS2 were aligned precisely to superpose the reconstructed images with high accuracy on the image plane.

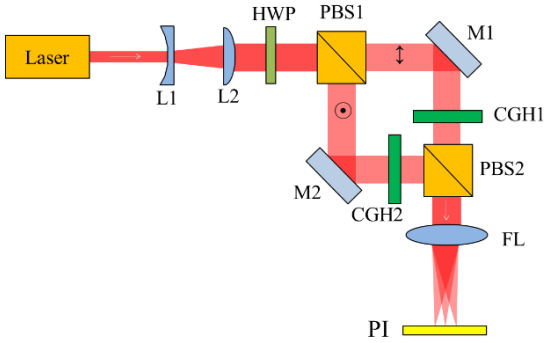

FIG. 4. Experimental setup for laser processing using two holograms. L: lens, HWP: half-wave plate, PBS: polarizing beam splitter, M: mirror, CGH: computer-generated hologram, FL: f-theta lens, PI: polyimide.

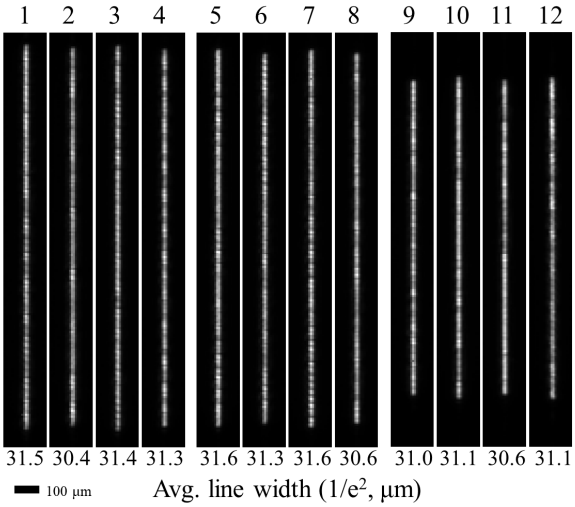

FIG. 5. Optically reconstructed line images. For each image, the top number is the line number defined in Fig. 3(b), and the bottom number is the average line width.

Figure 5 shows the optically reconstructed and superposed line images. The images were continuous and imaged on the flat plane without field curvature, as shown by the average line widths in Fig. 5. The processing target (polyimide film, 25.4 ± 1.3 μm thick) was located on the image plane. To firmly hold the target flat, its four sides were taped onto the aluminum plate with a beam path perforated. The required *z*-axis positional accuracy of the target was known to be less than the Rayleigh length [27], which was about 0.50 mm in this experiment. To find the optimal *z*-position for the target, we tested it at intervals of 0.10 mm, and we provide the result at the position having the narrowest kerf width.

4.2. Experimental Results

The incident pulse energy was 300 mJ on PBS1 and 150 mJ on each CGH, and the number of pulses used for drilling was 100 shots. Figure 6 shows the microscopic images of the results, featuring the continuously cut kerf for the entire area. Table 1 shows the average kerf width for each line; the total average was 20.0 ± 5.7 μm. Based on the energy irradiated on the sample and the reconstructed images of Fig. 5, we have calculated a fluence of 40.9 ± 8.0 J/cm^2 along the line center.

To ensure the superposition of orthogonally polarized images, laser drilling using a single CGH was performed with the same setup as the one in Fig. 4, except that one of the beams was blocked. Figure 7(a) shows one of the reconstructed line images, while Fig. 7(b) shows one of the laser-drilling results using a single CGH. As the result shows, the spots were not connected to each other, showing discontinuity, and only 64% of the total length was cut.

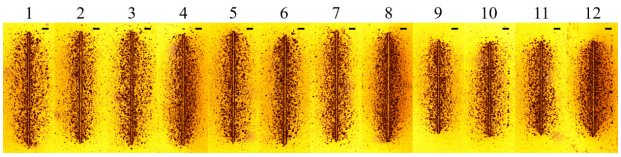

FIG. 6. Microscopic images of the processing results using two CGHs. The top numbers are the line numbers defined in Fig. 3(b). In each panel, the small black scale bar is 100 μm long.

TABLE 1. Average kerf width of the processing results for each line (μm)

16.7 ± 5.6	22.0 ± 5.8	19.3 ± 5.0	19.9 ± 5.1
20.8 ± 5.9	22.0 ± 4.9	20.3 ± 6.2	23.5 ± 4.5
19.5 ± 4.5	17.2 ± 5.6	17.7 ± 5.1	20.6 ± 5.7

The processing results showed the inhomogeneity of the kerf width, and randomly distributed damaged spots occurred around the kerf (about 400 μm in width at the line center), which is called the heat-affected zone (HAZ). We compared these to a processing result for a uniform line produced by a cylindrical lens. Figure 8(a) shows a focused line image produced with the cylindrical lens. Both ends were truncated to match the length of the reconstructed line images produced with the CGHs, and it had a similar line width of 36.0 μm. The experiment was performed with the same laser conditions (wavelength, pulse width, and repetition rate). The fluence at the line center was 45.3 ± 1.6 J/cm^2. Its mean value was adjusted as closely as possible to that of the previous experiment, and the standard deviation was significantly lower, due to the uniformity of the lines. The number of shots was 100, which is the same as before. Figure 8(b) shows the experimental result for the cylindrical lens; its kerf width was 26.0 ± 3.8 μm. The average kerf width was larger for the cylindrical lens because of the larger linewidth and the higher fluence. Also, the ratio of the standard deviation to the average value showed better processing quality when using a cylindrical lens. Considering that the cylindrical lens showed more uniform line image intensity than the CGHs, it can be seen that the fluctuating intensity from fabrication errors of the CGHs caused quality degradation. In addition, because there was also some degree of inhomogeneity in the results of processing with a cylindrical lens, inadequate wavelength and pulse width for polyimide film can also be seen as factors in quality degradation.

Both of the above experiments show the HAZ, and it can be concluded that the reconstruction by the CGHs was not the main cause of the HAZ. There are several causes of the HAZ, a major cause of HAZ is the wavelength and pulse width of the laser, which are in the range where thermal processing is dominant. At a wavelength of 1064 nm, the photon energy is too low to break the polymer's bonds [28], and the pulse width of 10 ns is considerably longer than the electron-photon coupling time [29]. Therefore, the laser can be considered a heat source, and the absorbed heat energy is diffused, causing damage beyond the irradiated area. Such an HAZ may be suppressed by nonthermal processing using a UV laser or an ultrashort-pulse laser [30]. In addition, the polyimide film has a low absorption rate at the corresponding wavelength, which causes a large fluence, which also contributes to the HAZ.

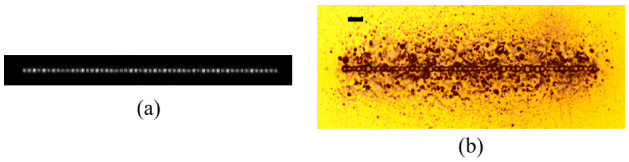

FIG. 7. (a) One of the optically reconstructed line images using a single CGH. (b) Microscopic image of the processing result using a single CGH. Scale bar: 100 μm.

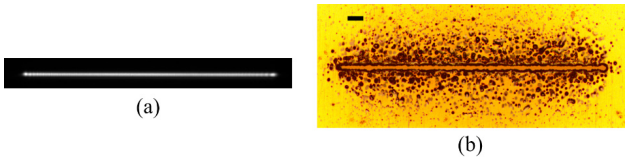

FIG. 8. (a) The optically reconstructed line images using a cylindrical lens. (b) Microscopic image of the processing result using a cylindrical lens. Scale bar: 100 μm.

V. DISCUSSION

For this method to be fully utilized as laser cutting, a laser with a pulse energy of several joules or more is required. For example, using the Spectra-Physics Quanta-Ray Pro-290 (maximum pulse energy 2 J), we expect to be able to cut patterns 130 mm in length under the same processing conditions (fluence, kerf width, etc.) as in this paper.

One of the patterns for effectively implementing the proposed method is singulation of a micro-SD card [31]. Unlike the target pattern of this paper, which consists of straight lines, the micro-SD card's pattern has a complex line image 52 mm in length, with diagonal and curved lines as well as vertical and horizontal ones. For simulation, we divided the spots alternately along the cutting line of the micro-SD-card target into two targets, to avoid interference noise. Figure 9(a) shows the simulated image when the orthogonally polarized images from divided targets are reconstructed and superposed. This simulation was intended to demonstrate feasibility, and was performed with a reduced pattern, compared to the actual micro-SD card. Figures 9(b)~9(d) show the images before and after superposition, for the portion containing lines in various directions. For diagonal components with an interval of 1.414 pixels, the line intensity was weaker than for a vertical or horizontal line with a 1-pixel interval. Therefore, to compensate for this, the CGHs were designed so that the spots of the diagonal components had higher intensity, about 1.3 times that of a vertical or horizontal line, so that they had a uniform intensity along the line after superposition.

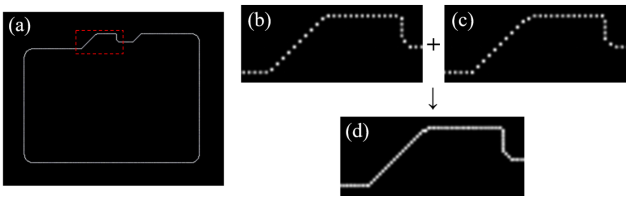

FIG. 9. (a) Simulated image of a micro-SD card reconstructed by superposition of orthogonally polarized images. (b,c) Simulated images of the micro-SD card before superposition, for the red square in (a). (d) Enlarged image of the red square in (a).

Considering that an actual micro-SD card has a perimeter of 52 mm, it was calculated that a pulse energy of approximately 0.7 J is required if we use image line width (~30 μm) and fluence (~40 J/cm^2) similar to those in the experiment performed in this paper. Actual values may be changed, considering that the material of a micro-SD card is epoxy and its thickness is 1.0 mm, and of course an experiment to find the appropriate wavelength and pulse width should be conducted.

VI. CONCLUSION

In conclusion, we have demonstrated nonscanning 2D laser drilling with arrays of closely spaced spots using two CGHs. To achieve this, the specklelike interference pattern was reduced by superposing two orthogonally polarized images, and the CGHs were fabricated with fused silica, which has a high damage threshold and can withstand high energy. Using the two CGHs and a pulsed laser, we successfully performed 2D laser drilling of polyimide film without a scanning process. This technique can be applied to 2D images of any shape, and enables a high-energy laser to be efficiently used for laser processing with high throughput. The processing results showed inhomogeneous kerf width, and a HAZ consisting of damage spots due to the thermal processing. We expect that higher quality can be achieved using advanced fabrication of CGHs, and a laser of shorter wavelength or shorter pulse width, with this verified technique.

ACKNOWLEDGMENT

This work is sponsored by the Civil Military Technology Cooperation Center (CMTC) of Korea under contract 12-DU-EN-01.

REFERENCES

1. D. Belforte, *Industrial lasers continue solid revenue growth in 2016* (Industrial Laser Solutions for Manufacturing, 18 Jan 2017), https://www.industrial-lasers.com/micromachining/article/16485081/industrial-lasers-continue-solid-revenue-growth-in-2016 (5 Oct 2017).
2. A. Salama, L. Li, P. Mativenga, and A. Sabli, "High-power picosecond laser drilling/machining of carbon fibre-reinforced polymer (CFRP) composites," Appl. Phys. A **122**, 73 (2016).
3. M. Vala and J. Homola, "Multiple beam interference lithography: A tool for rapid fabrication of plasmonic arrays of arbitrary shaped nanomotifs," Opt. Express **24**, 15656-15665 (2016).
4. K. Miyazaki, G. Miyaji, and T. Inoue, "Nanograting formation on metals in air with interfering femtosecond laser pulses," Appl. Phys. Lett. **107**, 071103 (2015).
5. P. S. Salter and M. J. Booth, "Addressable microlens array for parallel laser microfabrication," Opt. Lett. **36**, 2302-2304 (2011).
6. J. Kato, N. Takeyasu, Y. Adachi, H.-B. Sun, and S. Kawata, "Multiple-spot parallel processing for laser micronanofabrication," Appl. Phys. Lett. **86**, 044102 (2005).
7. Z. Kuang, W. Perrie, D. Liu, P. Fitzsimons, S. P. Edwardson, E. Fearon, G. Dearden, and K. G. Watkins, "Ultrashort pulse laser patterning of indium tin oxide thin films on glass by uniform diffractive beam patterns," Appl. Surf. Sci. **258**, 7601-7606 (2012).
8. Y. Jin, W. Perrie, P. Harris, O. J. Allegre, K. J. Abrams, and G. Dearden, "Patterning of Aluminium thin film on polyethylene terephthalate by multi-beam picosecond laser," Opt. Lasers Eng. **74**, 67-74 (2015).
9. S. Hasegawa, H. Ito, H. Toyoda, and Y. Hayasaki, "Massively parallel femtosecond laser processing," Opt. Express **24**, 18513-18524 (2016).
10. K. L. Wlodarczyk, M. Ardron, N. J. Weston, and D. P. Hand, "Holographic watermarks and steganographic markings for combating the counterfeiting practices of high-value metal products," J. Mater. Process. Technol. **264**, 328-335 (2019).
11. P. Kunwar, L. Turquet, J. Hassinen, R. H. A. Ras, J. Toivonen, and G. Bautista, "Holographic patterning of fluorescent microstructures comprising silver nanoclusters," Opt. Mater. Express **6**, 946-951 (2016).
12. K. L. Wlodarczyk and D. P. Hand, "Shaping the surface of Borofloat 33 glass with ultrashort laser pulses and a spatial light modulator," Appl. Opt. **53**, 1759-1765 (2014).
13. T. Häfner, J. Heberle, D. Holder, and M. Schmidt, "Speckle reduction techniques in holographic beam shaping for accurate and efficient picosecond laser structuring," J. Laser Appl. **29**, 022205 (2017).
14. L. Büsing, S. Eifel, and P. Loosen, "Design, alignment and applications of optical systems for parallel processing with ultra-short laser pulses," Proc. SPIE **9131**, 91310C (2014).
15. J. J. J. Kaakkunen, P. Laakso, and V. Kujanpää, "Adaptive multibeam laser cutting of thin steel sheets with fiber laser using spatial light modulator," J. Laser Appl. **26**, 032008 (2014).
16. C. Mauclair, D. Pietroy, Y. Di Maio, E. Baubeau, J.-P. Colombier, R. Stoian, and F. Pigeon, "Ultrafast laser microcutting of stainless steel and PZT using a modulated line of multiple foci formed by spatial beam shaping," Opt. Lasers Eng. **67**, 212-217 (2015).
17. K. S. Hansen, F. O. Olsen, M. Kristiansen, and O. Madsen, "Joining of multiple sheets in a butt-joint configuration using single pass laser welding with multiple spots," J. Laser Appl. **27**, 032011 (2015).
18. J. W. Goodman, "Some fundamental properties of speckle," J. Opt. Soc. Am. **66**, 1145-1150 (1976).
19. B. C. Kress and P. Meyrueis, *Applied Digital Optics: From Micro-Optics to Nanophotonics* (John Wiley & Sons, London, UK, 2009).
20. L. Golan and S. Shoham, "Speckle elimination using shift-averaging in high-rate holographic projection," Opt. Express **17**, 1330-1339 (2009).
21. J. Amako, H. Miura, and T. Sonehara, "Speckle-noise reduction on kinoform reconstruction using a phase-only spatial light modulator," Appl. Opt. **34**, 3165-3171 (1995).

22. Y. Takaki and M. Yokouchi, "Speckle-free and grayscale hologram reconstruction using time-multiplexing technique," Opt. Express **19**, 7567-7579 (2011).
23. M. Makowski, "Minimized speckle noise in lens-less holographic projection by pixel separation," Opt. Express **21**, 29205-29216 (2013).
24. H. Lee, S. Park, B. G. Jeon, and H. J. Kong, "Reconstruction of static line images with reduced speckle using interlaced holograms for holographic laser cutting," Appl. Phys. B **122**, 192 (2016).
25. J. Bengtsson, "Kinoform design with an optimal-rotation-angle method," Appl. Opt. **33**, 6879-6884 (1994).
26. M. T. Gale, M. Rossi, J. Pedersen, and H. Schuetz, "Fabrication of continuous-relief micro-optical elements by direct laser writing in photoresists," Opt. Eng. **33**, 3556-3567 (1994).
27. I. Alexeev, J. Strauss, A. Gröschl, K. Cvecek, and M. Schmidt, "Laser focus positioning method with submicrometer accuracy," Appl. Opt. **52**, 415-421 (2013).
28. J. Meijer, "Laser beam machining (LBM), state of the art and new opportunities," J. Mater. Process. Technol. **149**, 2-17 (2004).
29. K. C. Phillips, H. H. Gandhi, E. Mazur, and S. K. Sundaram, "Ultrafast laser processing of materials: a review," Adv. Opt. Photonics **7**, 684-712 (2015).
30. R. Schaeffer, *Fundamentals of laser Micromachining* (CRC press, Boca Raton, USA, 2012), Chapter 2.
31. S. Jiang, "ASJ singulating micro SD cards," in *Proc. 2009 American WJTA Conference and Expo* (Waterjet Technology Association, Texas, Aug, 2009). Vol. 2, Paper A.